sure the plausible extrapolation of the reconstructed surface into unconstrained regions.
9. D. J. Struik, *Lectures on Classical Differential Geometry* (Dover, New York, ed. 2, 1988).
10. Estimates of nonshape parameters include an independent value for the rotation period ($P = 4.07 \pm 0.03$ hours) and refined values for the time delay τ and 2380-MHz Doppler frequency ν of hypothetical echoes from Castalia's center of mass. These values were received at the center of curvature of the Arecibo telescope's main reflector, at the epoch 22 August 1989 06:45:00 UTC: $\tau = 37{,}453{,}066.9 \pm 0.3$ μs and $\nu = 173{,}116.5 \pm 0.1$ Hz.
11. The Castalia data apparently require a waist with severe surface curvature. The rippled appearance of the low-β_C, one-component models in Fig. 2A is an artifact, called Gibbs' phenomenon, of trying to use a truncated series to represent a sharply curving, nearly discontinuous function. The two-component model avoids this drawback.
12. Removing the "dynamical" penalty functions $A(\mathbf{p})$ and $B(\mathbf{p})$ and allowing the nominal model to reconverge decreased χ^2 by less than 0.1%.
13. For the nominal model, estimates of the scattering-law exponent and reflectivity (see Eq. 5) are $n = 2.8 \pm 0.3$ and $\rho = 0.30 \pm 0.03$, where the uncertainties encompass values for the upper and lower bound models. The most commonly used measure of a radar target's reflectivity is the radar albedo $\hat{\sigma} = \sigma/A_p$, which is the target's radar cross section divided by its projected area. Castalia's model albedo, averaged over all 64 frames, is 0.12 ± 0.01. A sphere with Castalia's values for ρ and n would have a radar albedo $\hat{\sigma} = 2\rho/(n + 1) = 0.16 \pm 0.01$; this "equivalent spherical albedo" may permit more useful comparisons with other radar targets.
14. M. J. S. Belton *et al.*, *Science* **257**, 1647 (1992).
15. P. C. Thomas, *Icarus* **77**, 248 (1989).
16. For a single-δ observation, if δ is replaced by $-\delta$ and the model is replaced by its mirror image through the equatorial plane, then $\sigma_m(\tau,\nu;\psi)$ is unchanged. The spin vector's sign (that is, the sense of rotation) and its azimuthal coordinate could have been constrained if other radar-target directions had been sampled.
17. This research was conducted at Washington State University and the Jet Propulsion Laboratory, California Institute of Technology, under contract with the National Aeronautics and Space Administration.

30 September 1993; accepted 6 January 1994

The Cosmological Kibble Mechanism in the Laboratory: String Formation in Liquid Crystals

Mark J. Bowick,* L. Chandar, E. A. Schiff, Ajit M. Srivastava

The production of strings (disclination lines and loops) has been observed by means of the Kibble mechanism of domain (bubble) formation in the isotropic-nematic phase transition of the uniaxial nematic liquid crystal 4-cyano-4′-*n*-pentylbiphenyl. The number of strings formed per bubble is about 0.6. This value is in reasonable agreement with a numerical simulation of the experiment in which the Kibble mechanism is used for the order parameter space of a uniaxial nematic liquid crystal.

Symmetry-breaking phase transitions in nature often spawn topological defects. An example of such defects from condensed matter physics is vortices produced when helium is cooled through its superfluid phase transition. An important proposal from cosmology is that the observed structure of the universe contains relics of topological defects formed as the early universe cooled. The important question of the density of defects was first treated theoretically by Kibble (*1*) using a model in which the phase transition proceeds by the formation of uncorrelated domains that subsequently coalesce, leaving behind defects. A domain is a uniform region of the ordered, or low-temperature, phase. Kibble assumed that the order varied randomly from one domain to the next and smoothly in between, and so proposed a straightforward statistical procedure for calculating the probability of string formation.

Although the Kibble mechanism was proposed for cosmic domains and strings, it should also describe the formation of strings or line defects in laboratory systems. Some time ago, Zurek (*2*) suggested the examination of vortex formation in liquid helium. The first experimental success, however, came in research by Chuang and co-workers (*3, 4*). Working with nematic liquid crystals, these researchers were able to observe the evolution of line defects. In the present work, we report an experimental verification of a crucial aspect of the Kibble mechanism: String formation can be predicted statistically from domain coalescence. Experiments have also been reported recently on vortex line creation in liquid ^{4}He (*5*).

Nematic liquid crystals (NLCs) consist of rod-like molecules; the rods are randomly oriented in the isotropic, high-temperature phase but show long-range alignment in the nematic, orientationally ordered phase (*6*). To quantitatively distinguish the ordered and disordered phases, an order parameter is typically introduced. For NLCs, this parameter may be taken to be the mean orientation of rods. This value is zero in the isotropic phase and nonzero in the nematic phase. Orientational order in the nematic phase is described by a unit three vector $\mathbf{n}$ without sign, because there is no preferred polarity to the constituent rods ($\mathbf{n} \equiv \mathbf{n}$). Thus, the space of possible nematic ground states is the two-sphere S^2, with opposite points of the sphere regarded as the same (*7*). This space is rich in topological defects (*6–11*). It has point-like defects (monopoles), line defects (disclinations or strings), and three-dimensional defects (texture).

Before describing the present work with NLCs, we illustrate the Kibble mechanism using string formation for the simpler case of two spatial dimensions (planar spins) (*8*). The order parameter in some small spatial region is a unit vector with orientation θ varying between 0 and 2π (the ground-state manifold is a circle S^1). If we follow θ along a closed path, we can determine the total angle $\Delta\theta$ by which θ winds; of course $\Delta\theta$ must be some integer multiple of 2π. When $\Delta\theta$ is nonzero, a defect must be present inside the path (see Fig. 1A).

Consider now the situation when three randomly oriented domains meet at a point (Fig. 1B). We can then calculate the winding angle $\Delta\theta$ using a closed path that circulates in some specified direction around the intersection point; the dashed line in the figure illustrates such a path. If $\Delta\theta = +2\pi$, one type of elementary string is formed when the three domains coalesce.

The probability of string occurrence is

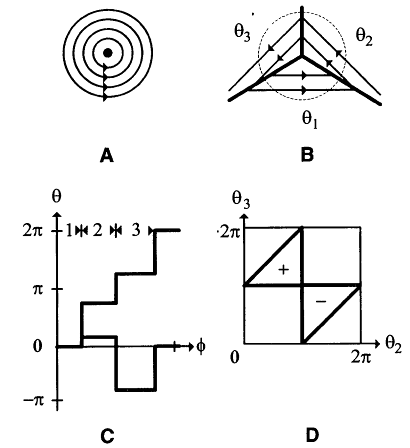

Fig. 1. A series of four diagrams illustrating the Kibble mechanism for planar spins. (**A**) The concentric circles indicate field lines of the order parameter and require an elementary topological defect at the origin. (**B**) Three domains with uniform order parameters θ_1, θ_2, and θ_3. The dashed circle indicates a loop around which a winding angle $\Delta\theta$ is calculated. (**C**) A graph illustrating the calculation of the winding angle for a path through three domains such as in (B). By definition, $\theta_1 = 0$. The jumps in θ between domains are minimized: This is the geodesic rule. Two different sets of order parameters are shown; the upper curve leads to defect formation ($\Delta\theta = +2\pi$), and the lower curve does not ($\Delta\theta = 0$). (**D**) The triangles labeled (+) and (−) indicate the combinations of θ_2 and θ_3 leading to $\Delta\theta = \pm 2\pi$ defects. One-fourth of all combinations lead to defect formation.

M. J. Bowick, L. Chandar, E. A. Schiff, Department of Physics, Syracuse University, Syracuse, NY 13244–1130, USA.
A. M. Srivastava, Institute for Theoretical Physics, University of California, Santa Barbara, CA 93106, USA.

*To whom correspondence should be addressed.

easily calculated. We denote the order parameters in the three domains as $\theta_1 = 0$, θ_2, and θ_3. We wish to calculate the winding angle $\Delta\theta$; the sequence of domains follows the circulation of our path. We also assume that the variation in θ from one domain to the next is minimized. For example, in Fig. 1C the upper curve has $\theta_3 > \pi$. We then show θ rising up to $+2\pi$ at the wall between domains 3 and 1. A return to $\theta = 0$ is excluded because this would require a larger jump. In fact, for a string in which $\Delta\theta = +2\pi$, we must have $\theta_3 > \pi$. We must also require $\theta_3 - \pi < \theta_2 < \pi$. If this second inequality is violated, we get $\Delta\theta = 0$ instead, as shown in the lower curve. Allowing windings by $\pm 2\pi$, one can readily estimate the probability P of forming a defect from the geometrical construction of Fig. 1D, obtaining $P = 1/4$ (12).

The generalization to three dimensions of the point defect just described for planar spins is a line defect. Spin systems, however, do not possess such line defects. Here the ground-state manifold is a sphere S^2; unlike the circle S^1, closed paths on a sphere are topologically equivalent to points and do not indicate line defects. Nematic liquid crystals, on the other hand, do exhibit line defects, because the orientation is described by a vector with the added property that orientations $\mathbf{n}$ and $-\mathbf{n}$ are equivalent [this ground-state manifold is denoted as the coset S^2/Z_2, where Z^2 is the cyclic group of order 2 $(1, -1)$]) (8–11). A string defect in this case corresponds to the situation in which the director $\mathbf{n}$ rotates by π along a closed path; this is called a strength 1/2 defect. In two dimensions the Kibble prediction for the probability of defect formation for the manifold S^2/Z_2 can again be obtained analytically, yielding $1/\pi$ (13).

We now turn to our experiments and simulations. We studied the NLC *K*15 (4-cyano-4′-*n*-pentylbiphenyl; BDH Chemicals, Ontario). We used an Olympus model BH phase-contrast microscope, equipped with a monochrome television camera and a standard video cassette recorder. We placed a drop of *K*15 on a clean, untreated microscope slide and heated the drop with an illuminator. After a slow reduction of intensity, we were able to obtain clear images of bubble formation and evolution as the drop cooled through the isotropic-nematic (I-N) phase transition at 35.3°C.

One set of such images is reproduced in Fig. 2. Figure 2A shows the numerous small isolated bubbles of the nematic phase that form first. At short intervals later, the nematic bubbles increase in size (Fig. 2, B and C), both by natural growth and by coalescence. In the next stage, the organization of the NLC into bubbles is replaced by an image of a homogeneous medium with entangled strings (Fig. 2D), which further evolve by straightening, shrinking, and the excision of small loops of closed string (Fig. 2E). The associated string dynamics have been well described (3, 4). As time passes, the string pattern "coarsens."

An important aspect of these observations is that the nematic bubbles shown in Figs. 2, A to C, formed in a single sheet near the top of the liquid crystal droplet. The depth of field of our microscope was about 40 μm. We see no out of focus bubbles, nor do we see the shadowing of bubbles by other bubbles. We presume that the liquid crystal cooled most rapidly near the air interface, leading to the formation of a nematic sheet at this interface.

It is fairly straightforward in the examination of Fig. 2C to select a minimal, spherical bubble that may contribute to the observed string formation. Larger, oddly shaped bubbles arise from the coalescence of two or more minimal bubbles. We therefore estimate the total number of bubbles N for the image by counting the total number of minimal bubbles involved, with coalesced bubbles counted as the appropriate multiple. In Fig. 2C we find $N \sim 55$. This procedure is somewhat ambiguous, and we found about a 10% standard deviation in independent estimates of the bubble count in a given picture. This value is compatible with the standard deviation in the bubble count for different sequences.

We now proceed to estimate the expected number of strings per bubble n_s from the measured string length L_s in Fig. 2D and the bubble count N. The total string length is $L_s = n_s N d$, where d is the linear size of a minimal bubble. This size may be estimated as $d = \sqrt{A/N}$, where A is the area of the image in Fig. 2C. Thus, we find $n_s = L_s/\sqrt{AN}$. For Fig. 2C we measure $L_s \simeq 2.7$ mm, yielding $n_s \sim 0.61$. We repeated this analysis on three sequences, obtaining $n_s = 0.64 \pm 0.02$ for the average number of strings per bubble. The error here is the simple statistical error in the mean. Our true errors are dominated by the ambiguities in bubble count mentioned above and by the coarsening of strings between Figs. 2C and 2D, which reduces the string length.

We now estimate the probability of string formation in our experiment using an elaboration of the Kibble calculation described earlier. For this estimation, we need a model for the directors in a "raft" of nematic bubbles just before coalescence (Fig. 2C). We assume that the director orientation inside a given bubble is roughly uniform and that this overall orientation varies randomly from one bubble to another. The top portions of the bubbles are in contact with air. We also assume that the

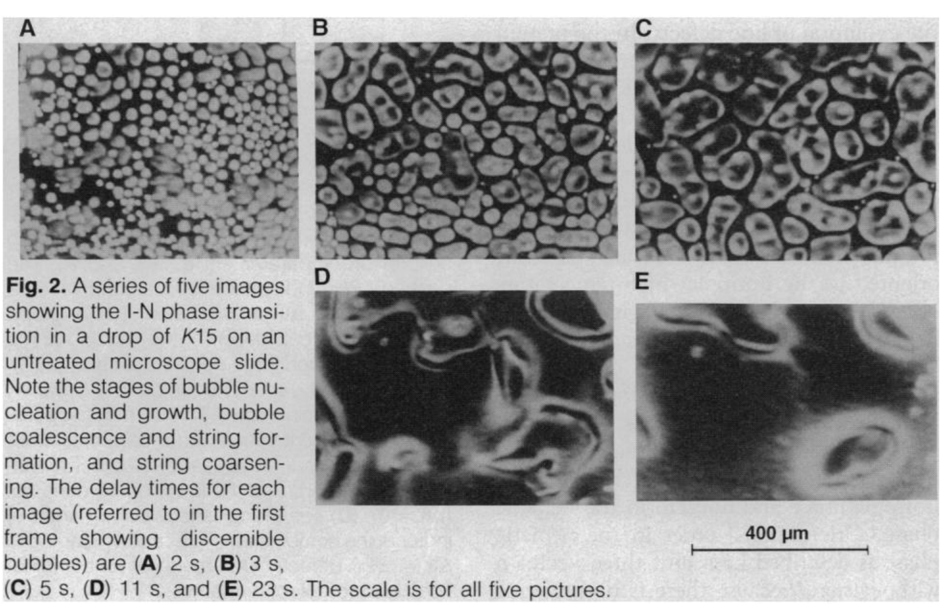

Fig. 2. A series of five images showing the I-N phase transition in a drop of *K*15 on an untreated microscope slide. Note the stages of bubble nucleation and growth, bubble coalescence and string formation, and string coarsening. The delay times for each image (referred to in the first frame showing discernible bubbles) are (**A**) 2 s, (**B**) 3 s, (**C**) 5 s, (**D**) 11 s, and (**E**) 23 s. The scale is for all five pictures.

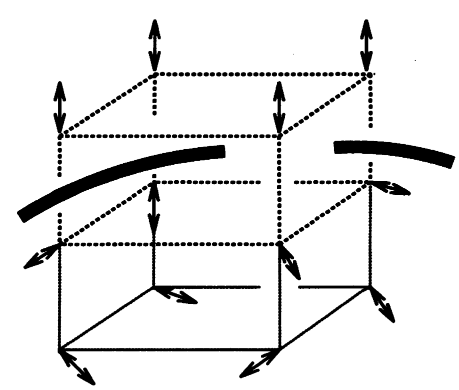

Fig. 3. Lattice representing the domain structure expected as the nematic bubbles coalesce. The top faces represent the nematic-air interface where the director is normal to the surface. The bottom faces correspond to the N-I interface where the director makes an angle of 63.5° from the vertical (although it can vary azimuthally). Middle lattice sites represent the regions near the centers of the bubbles.

director in each bubble near the air interface is vertical (9). Similarly, the bottom portion of each bubble is in contact with the isotropic phase, where measurements indicate that the director is anchored at an angle $\theta_{NI} = 63.5° \pm 0.6°$ from the vertical (*14–16*).

This configuration of directors is illustrated in Fig. 3. The two-headed arrows on each vertical dotted line represent the directors for the top, the bulk, and the bottom of a given bubble. After coalescence, the application of the geodesic rule for this configuration of directors is consistent with the emergence of a horizontal string, as indicated by the bold solid line. This model for string formation accounts for the observed absence of strings terminating at the interfaces. Strings certainly do not pass through the top, because the director orientation is constant everywhere. Although the director at the bottom sites can have some variation, no string can pass through the bottom faces. This limitation is because the entire bottom face (including the links) is supposed to represent the N-I interface where the director has fixed anchoring. For the bottom face, the geodesic rule is applied with this additional restriction on the director orientation. A little thought then reveals that a strength 1/2 line defect cannot pass through the bottom face of the lattice. Because in our experiment we only see the two-dimensional projected length of the string, we estimated the horizontally projected average length of the strings per bubble of unit size. We generated 50,000 random configurations of directors, consistent with the boundary conditions, and computed the corresponding value of n_s to be 1.564 ± 0.006 (*17*).

This model is in fair agreement with our observations—it accounts for the formation of strings that do not terminate at the upper and lower interfaces and for the magnitude of the string length. There are two primary deficiencies. First, the model predicts two layers of strings, upper and lower. We have no clear evidence for more than a single layer; we do not clearly observe one string passing beneath another without contact. Second, the predicted string length is about twice as great as that observed. This quantitative discrepancy may be partially explained by string interactions in the seconds that pass between our last clear image of bubbles and our first clear image of strings (see Fig. 2, C and D), but a model that more clearly accounts for a single layer would also reduce the discrepancy.

We can account well for the observed string length if we assume that our measurements are sensitive primarily to strings at the air-nematic interface. It is plausible that the coalescence of two nematic bubbles forms horizontal strings that are in effect squeezed toward the interfaces; we anticipate that the free energy of strings at the air-nematic interface is significantly lower than that for bulk strings, so that the formation of a mat of strings at this interface is favored. The disadvantage of this approach is that we did not clearly observe structures that would correspond to a string descending from the surface toward the N-I interface. We speculate that intercommutation (*3*) may have disconnected the strings leading down from the surface mat during the several seconds that passed between our last clear image of bubbles (Fig. 2C) and our first clear image of strings (Fig. 2D). In any event, we reanalyzed the simulation described earlier to estimate the horizontal length of just the strings in the top half of Fig. 3. This reconsideration yields $n_s = 0.636 \pm 0.004$—in excellent agreement with our measured value (*18*).

REFERENCES AND NOTES

1. T. W. B. Kibble, *J. Phys. A Gen. Phys.* **9**, 1387 (1976).
2. W. H. Zurek, *Nature* **317**, 505 (1985).
3. I. Chuang, R. Durrer, N. Turok, B. Yurke, *Science* **251**, 1336 (1991).
4. I. Chuang, N. Turok, B. Yurke, *Phys. Rev. Lett.* **66**, 2472 (1991).
5. P. C. Hendry, N. S. Lawson, R. A. M. Lee, P. V. E. McClintock, C. D. H. Williams, *Physica B*, in press.
6. P. G. de Gennes, *The Physics of Liquid Crystals* (Clarendon, Oxford, 1974).
7. Technically, the resultant space S^2/Z_2 is called the projective plane RP^2.
8. N. D. Mermin, *Rev. Mod. Phys.* **51**, 591 (1979).
9. Y. Bouligand, in *Les Houches Session XXXV, Physics of Defects*, R. Balian, Ed. (North-Holland, Dordrecht, Netherlands, 1981).
10. M. Kleman, *Points, Lines and Walls in Liquid Crystals, Magnetic Systems and Various Ordered Media* (Wiley, Chichester, 1983).
11. S. Chandrasekhar and G. S. Ranganath, *Adv. Phys.* **35**, 507 (1986).
12. The assumption of the least variation of θ used above is called the geodesic rule. The rule is a plausible consequence of minimizing the gradient energy associated with the spatial variation of θ.
13. T. Vachaspati, *Phys. Rev. D* **44**, 3723 (1991).
14. S. Faetti and V. Palleschi, *Phys. Rev. A* **30**, 3241 (1984).
15. A curious implication of the N-I boundary conditions is that an isolated nematic bubble should contain a monopole topological defect. This condition may not apply in sufficiently small bubbles [the so-called thick wall bubbles; for example, see (*16*)]; inside such bubbles the magnitude of the director is smaller than the value appropriate for the nematic phase (*16*).
16. A. M. Srivastava, *Phys. Rev. D* **45**, R3304 (1992); *ibid.* **46**, 1353 (1992).
17. We also checked the dependence of n_s on the anchoring angle θ_{NI} of the director at the N-I interface. For $\theta_{NI} = 0.0$, n_s is found to have a smallest value equal to 1.264. The number of strings per bubble increases monotonically with θ_{NI}, from $n_s = 1.34$ for $\theta_{NI} \simeq 30°$ to a maximum value of 1.628 for $\theta_{NI} = \pi/2$. This dependence of n_s on θ_{NI} is easy to understand because with increasing θ_{NI}, the allowed values for the director form a larger and larger set (which leads to a larger n_s for a cubic lattice), with the largest set attained at $\theta_{NI} = \pi/2$.

18. We thank M. Hindmarsh, P. Palffy-Muhoray, G. Ranganath, C. Rosenzweig, and B. Yurke for discussions and E. Lipson for making these experiments possible. Supported by U.S. Department of Energy (DOE) grant DE-FG02-85ER40231 (to M.J.B.) and by National Science Foundation grant PHY89-04035 and DOE contract DE-AC02-83ER40105 at the University of Minnesota (to A.M.S.).

13 October 1993; accepted 3 December 1993

Laser-Based Analysis of Carbon Isotope Ratios

D. E. Murnick* and B. J. Peer†

A laser technique for analysis of carbon-13 : carbon-12 ratios with the specificity of laser resonance spectroscopy and the sensitivity and accuracy typical of isotope ratio mass spectrometers is reported. The technique is based on laser optogalvanic effect spectroscopy, in which an electrical (galvanic) signal is detected in response to the optical stimulation of a resonance transition in a gas discharge species. Carbon dioxide molecular gas lasers are used, with the probed transitions being identical to the lasing transitions. Measurements for carbon dioxide samples with 100-second averaging times yield isotopic ratios with a precision of better than 10 parts per million.

Carbon isotopic analysis is an important tool in geology (*1*), environmental science (*2*), biology (*3*), and medicine (*4*). In geological studies, such as the sedimentation of carbonates, or in atmospheric studies, such as polar ice core and oceanic isotope measurements, it is the $^{13}CO_2 : ^{12}CO_2$ ratio that is of primary importance in the determination of the cycle of CO_2 production and absorption throughout history. In biological and medical studies, analysis of isotopic carbon ratios makes possible the study of metabolic pathways in living systems. Presently, either the radioactive tracer ^{14}C or stable ^{13}C is used for such analysis. The use of ^{13}C as a tracer for diagnostic purposes is a rapidly growing field (*5*). The use of stable ^{13}C rather than the radioactive isotope ^{14}C obviates potential harmful radiation effects and eliminates time constraints and the problem of radioactive waste disposal.

Department of Physics, Rutgers University, Newark, NJ 07102, USA.

*To whom correspondence should be addressed.
†Present address: Department of Geology and Planetary Science, University of Pittsburgh, Pittsburgh, PA 15260, USA.